Long-term forecast of oceanic conditions off California and their biological implications

Guillermo Auad,[1] Arthur Miller,[1] and Emanuele Di Lorenzo[1,2]

[1]   The impact of global warming due to an increased content of atmospheric CO_2 is studied by forcing a numerical eddy-resolving ocean model with wind stresses, heat fluxes, and open boundary conditions obtained from a state-of-the-art coupled model. Specifically, we have compared the 1986–1996 and 2040–2050 decades to describe and analyze the changes attained by several oceanographic variables in the California Current System. A richer atmosphere in CO_2 leads to increased sea surface and near-surface temperatures in the model domain and to an increased stratification along the coast that, however, is not strong enough to overcome the effect of increased upwelling favorable winds. A mild oceanic cooling is forecast below the 70-m depth, in agreement with recent studies of global warming trends. Near-surface vertical velocities increase by about 30% in April, but our simulations also forecast anomalous offshore transports in most of the coastal areas. The eddy kinetic energy decreases, on an annual mean, along the California Current main path with maximum negative anomalies in winter. The upward displacement of the 26.5 isopycnal surface, especially in the northern half of our study area, leads to an increase in the concentration of nutrients in the subsurface. The agreement between some results of this forecasting study and recent published findings would suggest that the current global warming trend would persist in the study area with similar changes to those observed over the last half century.

1.   Introduction

[2]   The well-studied 1976–1977 warming shift [e.g., *Miller et al.*, 1994] had a well-defined impact on the dynamics and biology off the North Pacific eastern boundary. For instance, increased surface temperatures led to changes in the usual geographical distribution of zooplankton [*Roemmich and McGowan*, 1995], which in turn led to drastic recruitment changes in several commercial species as documented by *MacCall and Prager* [1988] and *Beamish* [1993]. This knowledge becomes very useful when trying to forecast the state of the ocean under the current global warming trend [*Hansen*, 1998], in particular when the study area is one of the most actively exploited and navigated regions in the world. Several commercial species are actively exploited in the California Current System area, for example, sardines (*Sardinops sagax*), anchovies (*Engraulis mordax*), and Pacific mackerel (*Scomber japonicus*), among others.

[3]   Both, observations [*Hickey*, 1979] and models [*Auad et al.*, 1991] show that the California Current System (CCS) can be described in terms of four components: the California Current (CC), the Davidson Current (DC), the California Undercurrent (CU), and the Southern California Eddy (SCE). However, these features attain active and continuous fluctuations in both, their position and intensity. It is the goal of this article to describe and explain the main climatological changes of the CCS, in space and time, when their external forcing experiences a sustained climatological change between 1991 and 2045. We will also compare the results obtained in this article to those obtained by other authors [*Bakun*, 1990; *Barnett et al.*, 2005] from observed and modeled trends estimated over the past few decades. For instance, do different warming scenarios, for example, regional and basin scale, lead to similar changes in the CCS?, does an abrupt warming shift (e.g., 1976–1977) lead to the same equilibrium state as a slow warming trend? Is the description of the global warming trend of the past 40 years similar to that one of the next 40 years?

[4]   In order to achieve a good spatial resolution, we defined a relatively small geographical domain. This is a first step in a series of papers aimed to investigate the impact of global warming on the whole eastern North Pacific. Future experiments, some underway, will include larger domains, and sea-ice models. This article is organized in the following manner: in section 2 we will describe the model and methodology, and in section 3 the results will be

---

[1]Scripps Institution of Oceanography, La Jolla, California, USA.
[2]Now at School of Earth and Atmospheric Sciences, Georgia Institute of Technology, Atlanta, Georgia, USA.

shown and described. Discussions and conclusions are left for section 4.

2. ROMS Model

[5] The Regional Ocean Model System (ROMS) is an s coordinate, terrain following, primitive equation model. It is an optimized version of SCRUM [*Song and Haidvogel*, 1994], modified to run in multiprocessor servers. The present configuration uses a 9-km horizontal resolution and 20 layers in the vertical. Radiation conditions for all, tracers (salinity and potential temperature), and barotropic and baroclinic velocity components are used at the open boundaries along with 54-km-wide sponge layer with maximum values of viscosity and diffusivity of 100 and 50 m^2 s^{-2}, respectively.

2.1. Runs' Forcing

[6] Three 10-year-long runs were carried out. The base run only includes climatological forcing for all, OBCs, wind stress and surface heat fluxes. The second run includes anomalous plus climatological wind stresses and OBCs, leaving local heat fluxes in their climatological values. The final run includes anomalous plus climatological forcing in all, OBCs, wind stress and heat fluxes. All runs include climatological freshwater forcing. The anomalous components for both forcing functions are obtained as follows. The climatological values of the 1986–1996 decade are subtracted from those of the 2040–2050 decade, and this difference is added to the former climatology. In this way, every year is identical to the others. The model is then run until reaching statistical equilibrium. To obtain the climatic change of a given variable, say sea surface temperature (SST), its value from the climatological run is subtracted from those of the anomalous run. In this manner, any linear drift common to both runs is removed since both runs start from the same initial conditions (climatological values). To analyze the output of every run, the first 3 years are ignored similarly to *Marchesiello et al.* [2003], who spun up their CCS ROMS equilibrium runs for 2 years. Here all averages are estimated using the last 7 years of each 10-year-long run. The volume-integrated kinetic energy shows a seasonal cycle and interannual variability as an indication of intrinsic variability.

[7] Climatological freshwater fluxes (precipitation, evaporation and river runoff) were included but anomalies were excluded since their contribution to climate changes, in any of the variables analyzed in this paper, is largely controlled by anomalous surface heat fluxes and wind forcing [e.g., *Miller et al.*, 1994; *Auad et al.*, 1998]. Global data sets [e.g., *Oberhuber*, 1988] (iridl.ldeo.columbia.edu) show precipitation minus evaporation values ranging between −30 and −25 mm month^{-1} in the CCS area. These are small values compared to those obtained in western boundary currents, typically of the order of 150–300 mm month^{-1}. No major river discharge exists in this region, although their contribution might become somewhat important north of our domain, from Oregon to Alaska, especially in the near-coastal ocean. *Dai and Trenberth* [2002] have estimated the freshwater discharge for the global ocean. From their study, annual discharge values into the CCS area are seldom over 0.6 m^3 s^{-1}, which is small compared to those found in the

Gulf of Alaska (4 m^3 s^{-1}) and in western Africa off the Angola's coast (20 m^3 s^{-1}).

[8] Climatological winds and freshwater fluxes are from the NCEP-NCAR reanalysis [*Kalnay et al.*, 1996], while climatological heat fluxes are from an updated analysis [*Cayan*, 1992] of the Comprehensive Ocean-Atmosphere Data Set (COADS). The anomalous components were obtained from the NCEP-NCAR regional spectral model (RSM) simulation downscaled from the ACPI Parallel Climate Model (PCM) global coupled model forecast runs described by *Han and Roads* [2004]. Their runs, used present-day and increased (36%) CO_2 concentration from the NCEP RSM [*Juang et al.*, 1997], and the PCM [*Washington et al.*, 2000]. The PCM is a coupled atmospheric ocean model capable of making historical and global change simulations. Its atmospheric component has a resolution T42 (about 280 km) and 18 vertical layers on a hybrid vertical coordinate. The ocean component has a resolution of 2/3° in midlatitudes, 1/2° in the tropics, 32 vertical levels and a free surface. The RSM in turn, has a horizontal resolution of 50 km. The PCM was then used to force the RSM at its boundaries every 6 hours. The boundaries of the RSM are far from the geographical boundaries of ROMS (at least 8°). To obtain ROMS' open boundary conditions (OBC) from the coupled PCM we used a cubic spline interpolation. This was similar to using linear interpolation since the PCM variables vary smoothly from grid point to grid point in the study area. Further details on their architecture are given by *Kanamitsu* [2000] and *Han et al.* [2000].

2.2. Climatological Changes in Atmospheric Forcing and OBCs

[9] The main changes in the wind stress forcing climatology are shown in Figure 1. In general the wind stress field anomaly shows an offshore increase of its amplitude and an inshore increase of its curl amplitude (Figure 2). In terms of directional changes, spring winds have a clear upwelling favorable component off central California. Offshore winds have a southward, year-round, component fluctuating between southwestward and southeastward depending on the specific location. In opposing contrast, the maximum wind stress curl changes are located nearshore, off central and northern California. This maximum amplitude rapidly decreases offshore and along the coast toward the south where changes are small. Upwelling events are reasonably resolved with a 9-km horizontal resolution [*Capet et al.*, 2004], although they showed that a more realistic model response is obtained when a horizontal resolution of 3 km is used.

[10] Surface net heat flux changes (not shown) warm up the ocean at every location in the study area, and this is mostly due to changes in the Newtonian cooling rate (i.e., the sensitivity of surface heat fluxes to changes in SST). Maximum values for the overall heat flux difference, between the 1990s and the 2040s, increase northward with values ranging between 20 and 40 W m^{-2}. However, sensible and latent heat flux changes are also positive in almost the whole domain but of smaller amplitude than the cooling rate. The spring season experiences the largest coastal warming from Baja California, in Mexico, to northern California. Model SSTs are relaxed to climatological
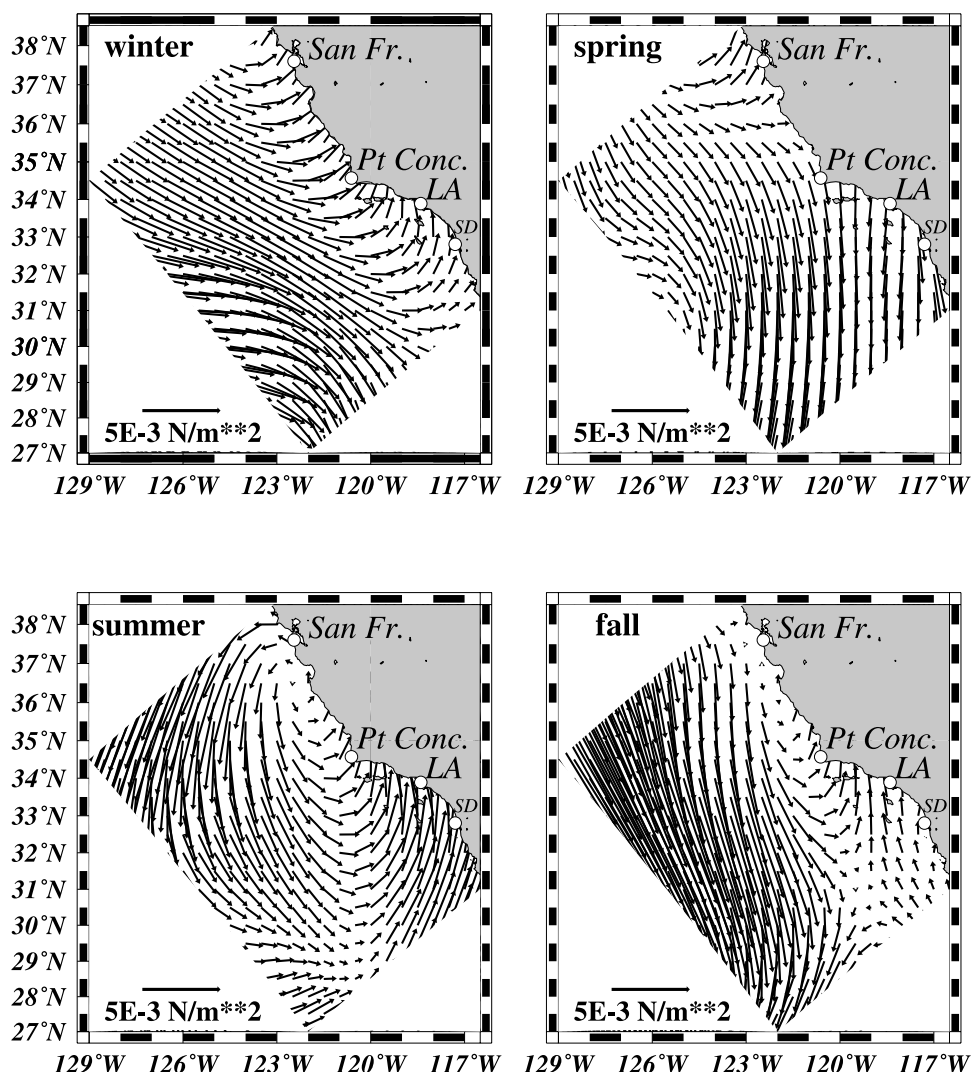
Figure 1. Climatological change in wind stress amplitude and direction between the 1986–1996 and 2040–2050 decades, as obtained from the RSM coupled model. The spring figure shows intensification in upwelling favorable winds.

SSTs from the COADS data set. No SSS relaxation was used in any of the runs, while Levitus climatologies [*Levitus et al.*, 1994] were used to obtain climatological initial conditions.

[11] The anomalous OBCs from the PCM have an into-the-domain flow, most of the year and at the surface, through the southern boundary, through the northern boundary and on the northernmost part of the western boundary. These directions of the anomalous flow are consistent with the spatial variations of the anomalous sea level if we invoke geostrophy. Seasonal variations for all variables are small, especially for temperature and salinity. Most of these anomalies attain very small values (always at the boundaries) below about 100 m for temperature and velocity and below 150 m for salinity. Temperature anomalies at the boundaries are characterized by positive values all along all three boundaries (and year-round) from the surface down to about 30–50 m. Salinity anomalies instead, attain negative values year-round and at all boundaries, from the surface down to depths ranging between about 100 and 400 m, depending on the location. Small positive anomalies are present always deeper than the negative ones in depths ranging from 100 to 300 m, for all seasons, with the only exception of the coastal area on the northern boundary where these positive salinity anomalies reach the surface (salinity anomalies for all boundaries and seasons range between −0.004 and 0.0004 psu).

3. Results

3.1. Oceanic Changes

[12] The main oceanic response to a CO_2-richer atmosphere in the 2040–2050 decade can be summarized as follows. A warmer atmosphere leads to a warmer upper ocean; this is mostly felt in the upper 50 m of the CCS. In contrast, near the coast, there is an increased positive wind stress curl, which favors an upward Ekman pumping velocity at the bottom of the mixed layer. The resulting picture is thus a warmer upper ocean with a very sharp thermocline with, despite the increased stratification, in-
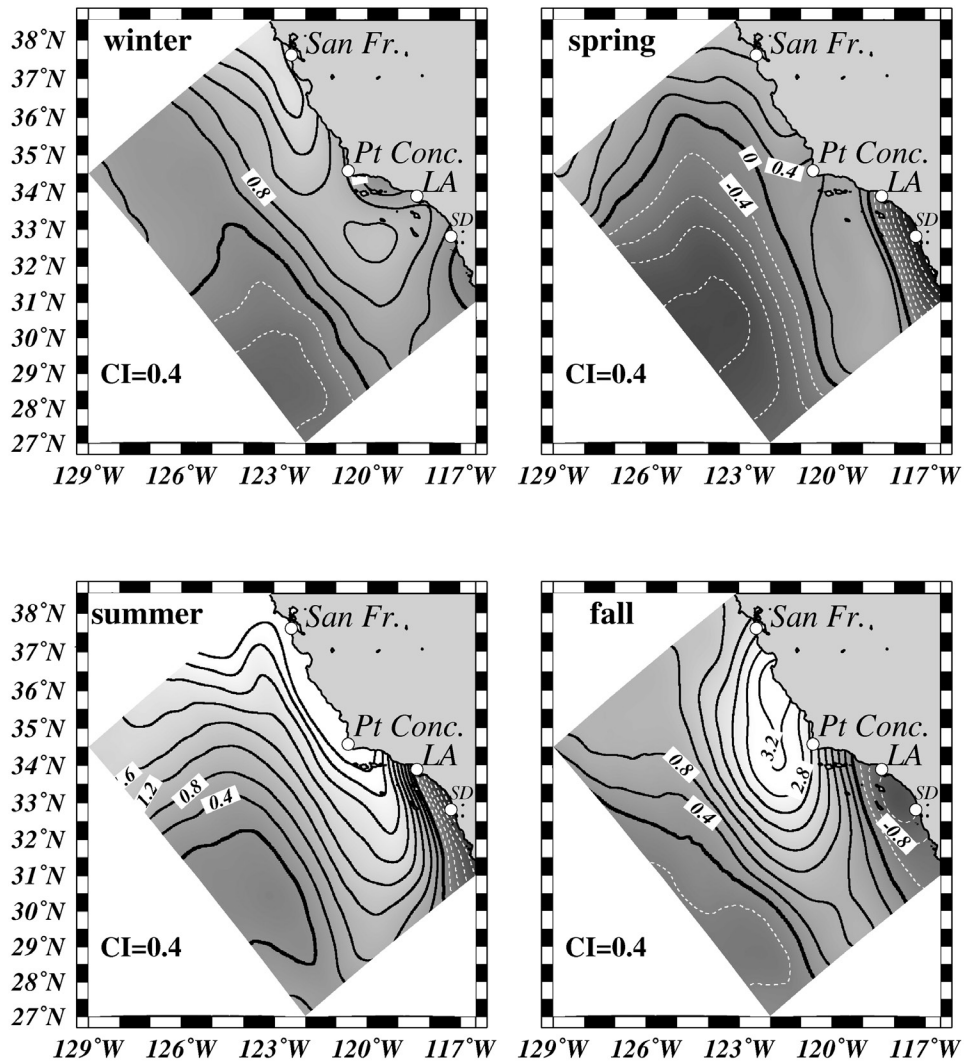
Figure 2. Climatological change in wind stress curl amplitude. Units are 10^{-8} N m^{-3}.

creased upwelling in spring. The California Current is accelerated by both, anomalous OBCs and by a wind stress-induced mass redistribution having maximum amplitude W to NW of Point Conception. South of this location, the CC is mildly slowed down while there is a forecast decrease in the eddy kinetic energy along the CC main path, also with maximum amplitudes in the northern half of the model domain. Almost all variables exhibit, on the mean, an active eddy field offshore, mainly all along the California Current path. This agrees with both historical observations [e.g., *Lynn and Simpson*, 1987; *Hickey*, 1979] and modeling experiments [e.g., *Auad et al.*, 1991], in the sense that an active eddy field largely controls the instantaneous surface flow of the CC along its NW to SE axis. In general, all variables exhibit their largest climatological changes in the northern half of our domain, i.e., north of Point Conception. Both, wind stress and heat flux climatological changes have maximum amplitudes in the northern half of the study area while anomalous OBCs have similar amplitudes at all locations for a given depth.

[13] Climatological changes in the depth of the 26.5 isopycnal are shown in Figure 3. Isopycnal depth anomalies become shallower in most of the study area in response to wind stress curl positive anomalies, also year-round (Figure 2), exhibiting a small seasonal variability with the largest amplitudes being induced in the northern half of the domain and offshore, in line with the observational analysis of *Palacios et al.* [2004]. The structure of this pycnocline deformation favors a geostrophic southward flow in the northwestern quadrant of our domain. Off central California, a geostrophic northward flow is supported by these anomalous density gradients, which tend to be largest in winter. A similar pattern was obtained for all seasons when no anomalous heat flux was used (not shown). Small positive anomalies tend to cover the southern half of the model domain while negative anomalies showed little variation in amplitude and location.

[14] A rather different picture is obtained from the ocean's response in sea level (Figure 4); for all seasons negative anomalies are seen offshore while positive ones are closer to the coast; this description did not hold when the
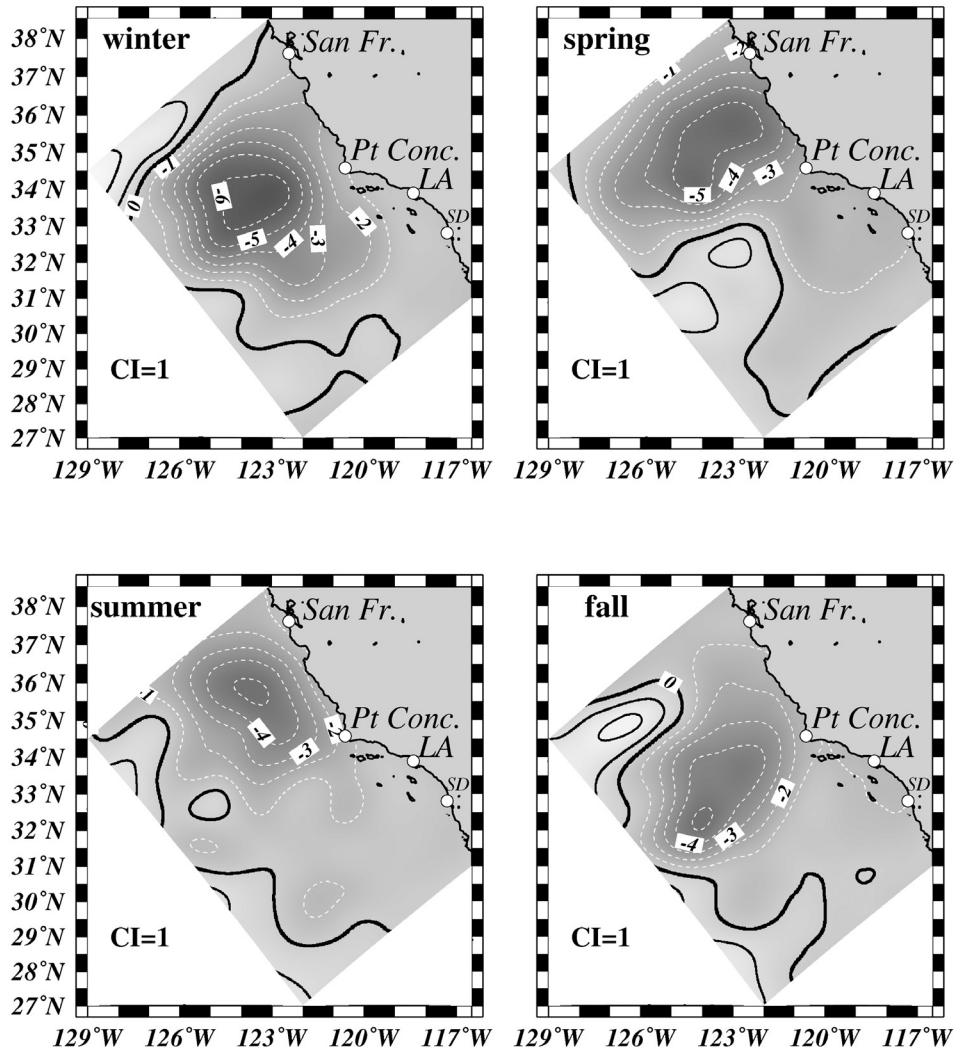
Figure 3. Climatological change in the depth of the $\sigma = 26.5$ kg m^{-3} isopycnal (meters). The model forcing included both heat fluxes and wind stresses.

model was forced with climatological heat fluxes only (not shown). Thus future sea level anomalies are strongly influenced by heat flux anomalies and favor the development of a geostrophic flow, which will tend to slow down the CC. In fact, the model's vertically averaged alongshore velocities (not shown) are northwestward although much weaker than the depth-dependant components in the upper 100 m. The positive sea level anomalies seen near the coast off San Diego are accompanied by underlying weak negative anomalies of isopycnal depth (Figure 3) which supports the idea that pycnocline depth anomalies are mainly controlled by wind stress field anomalies, while sea level changes are most responsive to the forcing induced by heat flux anomalies. As we will see in more detail, shallower isopycnals and a warmer surface layer lead to an increased stratification in the study area.

[15] Given the different wind regimes that characterize the CCS north and south of Point Conception [*Dorman and Winant*, 2000], we have computed the average temperature changes that take place north and south of this location

(excluding the coastal ocean), in order to compare with the recent results of *Barnett et al.* [2005]. The dividing line between north and south goes from Point Conception to the SW and normal to the western boundary of our domain. Figure 5 shows the climatological changes in temperature between the 1990s and the 2040s. The north and south halves of our offshore domain show warmer SSTs ranging between 0.3°C (winter, northern half) and 0.8°C (summer, northern half). The temperature anomalies change sign, depending on the season, and location, between 20 (summer, northern half) and 50 m (winter, southern half) with extreme cooling anomalies of −0.3°C taking place in the northern half and of −0.2°C in the southern half. These minimums, in both halves, take place at depths ranging between 60 and 70 m, while below 300 m anomalies are very small. These descriptions are in general good agreement with the recent values estimated by *Barnett et al.* [2005] from coupled model PCM simulations over the past 40 years (1960–2000). They computed vertical profiles of temperature averaged in the North Pacific where they
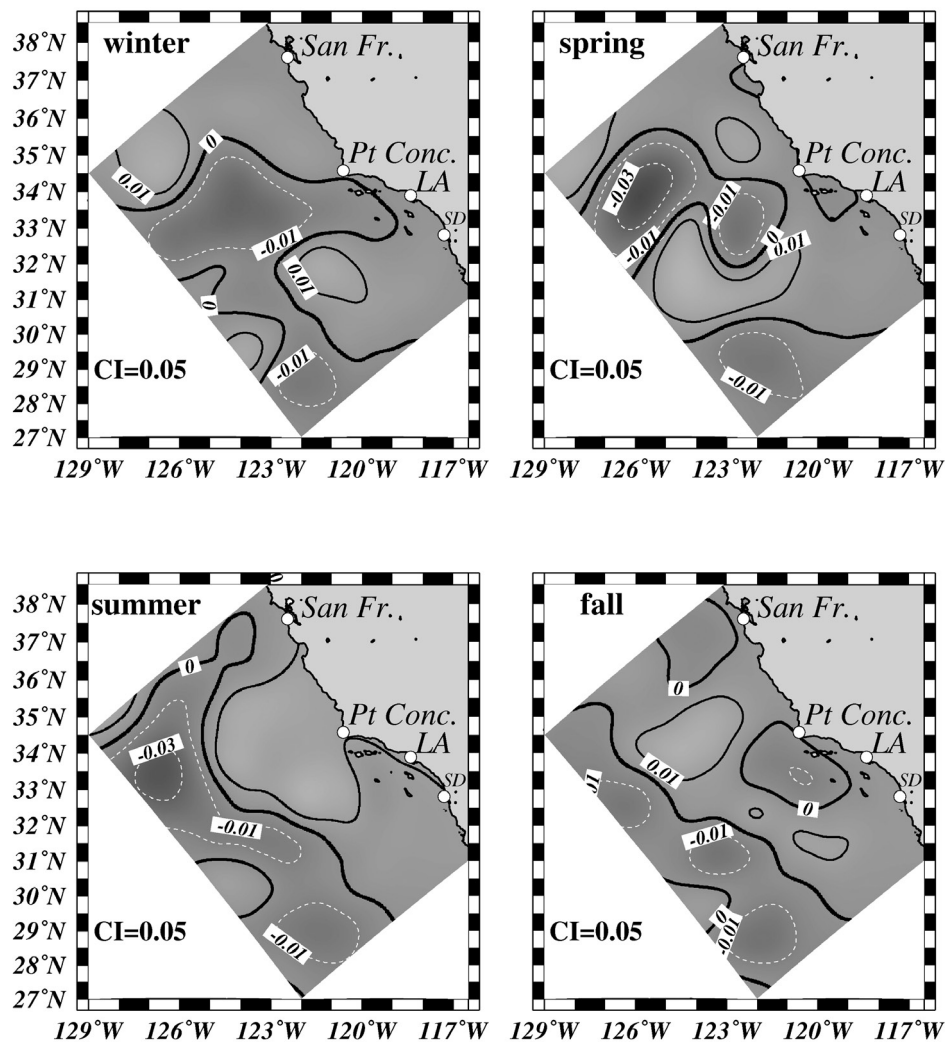
Figure 4. Climatological change in sea level height (meters).

describe a typical SST warming of 0.25°C, a change of sign at about 80 m and an extreme cooling of about 1.8°C at 150 m. As in our simulations, theirs also show very small anomalies (<0.05°C) below 300 m.

3.2. Biological Implications of Oceanic Climatological Changes

3.2.1. Climate Change in Alongshore Velocity Component

[16] This component of the total flow is responsible for advecting mean properties such as temperature and salinity since the strongest mean gradients are in the alongshore direction. The most salient climatological changes in the alongshore component of the flow at 150 m (i.e., to exclude Ekman currents) are (Figure 6): (1) the mild slow down of the CC in the southern half of the study area, on a annual average, and with maximum positive values along the coast and north of Point Conception in winter (i.e., accelerating the CU) and (2) a year-round acceleration of the mean flow of the CC in the northwestern part of the study area. The mean flow of the CC (not shown) enters the model domain

through its NW corner with its axis in the SSE direction then turning to the SEE at about 34°N. This acceleration, in the northern half of the domain, is fueled by both, anomalous OBCs (i.e., inflow) present at the western half of the northern boundary and at the northern half of the western boundary, and by the geostrophic flow induced by the climatological change in the isopycnal depths (Figure 3).

[17] The poleward anomalous coastal current at 150 m was also noticed at depth and intensified in winter, during the warming shift of 1976–1977 [*Auad et al.*, 2003], and during the termination of the last ice age 20,000 years ago [*Kennett et al.*, 2003]. This poleward current can have an important impact on the local ecosystem because it brings nutrient-rich waters into the CCS domain, which in turn can reach the surface during upwelling events. At this depth (150 m), changes in the alongshore flow are mainly controlled by changes in the mass distribution which are in turn governed by changes in the wind stress field. The last two referenced studies invoke basin-scale changes in the North Pacific Intermediate Water as a response to rapid atmospheric warming shifts. Whether the same occurs during
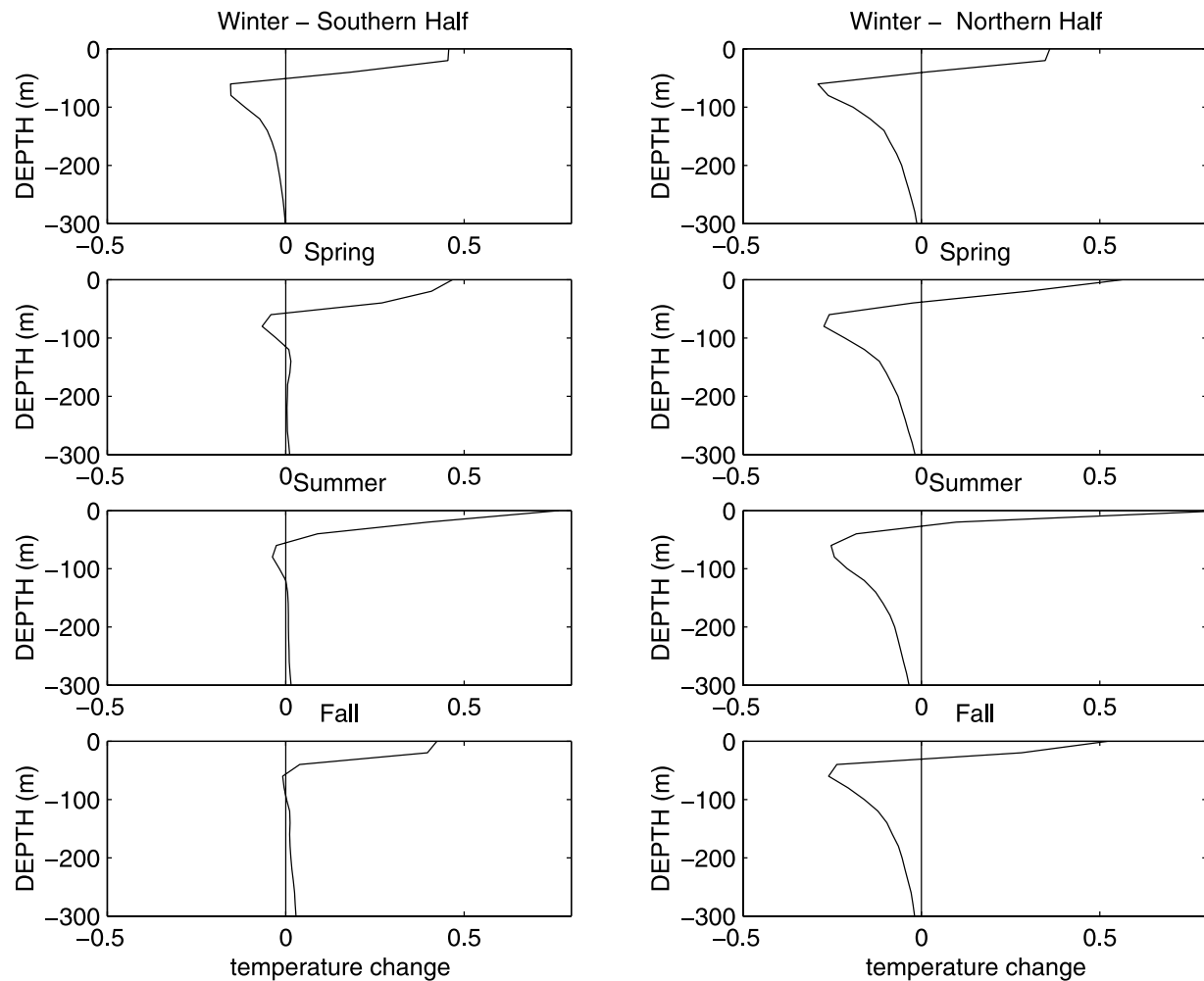
Figure 5. Climatological temperature changes for the (left) southern and (right) northern halves of the study area. The dividing line extends southwestward from Point Conception and normal to the western boundary. Averages excluded the 10 closest grid points (90 km) to the coastline.

slow warming trends, as in this study, is still an open question.

3.2.2. Climate Changes in the Acrosshore Velocity Component

[18] This biologically relevant variable is mostly controlled by climatological changes in the wind stress field. Its biological importance is simply dictated by its sign since it controls the offshore and onshore larvae transport. An onshore transport usually benefits the fish industry because fishing grounds are brought closer to the coast within operational reach for most fishing fleets. Since the dominant climatological component of the wind stress is in the alongshore direction, the acrosshore component of the surface flow is the one that reflects more strongly the wind stress forcing and its climatological differences. Changes in the acrosshore surface transport (Figure 7) are offshore almost year-round because of the prevailing changes in wind stress and hence in Ekman transport. The offshore portion of this area of positive anomalies is mostly due to geostrophic anomalies since the wind stress anomalies are normal to the coast there (Figure 1). Confirming this, the anomalous acrosshore flow at this location, from the surface

down to 150 m (not shown) is inshore. In summer, the inshore flow (positive anomalies) seen south of Los Angeles is mostly due to the Ekman transport induced by the wind stress anomalies of Figure 1. Typical climatological changes in the acrosshore flow are smaller than 2 cm s^{-1} in the coastal band and average 3 cm s^{-1} offshore, with the largest anomalies taking place in the northern half of the domain. The overall picture suggests, in the light of the study of *Watson* [1992], that there would be an increased offshore (or decreased inshore) year-round surface transport of Pacific sardine larvae north of Point Conception, and inshore south of Point Conception, especially in winter.

3.2.3. Climate Changes in Eddy Kinetic Energy

[19] Another important aspect with biological implications is the eddy kinetic energy (EKE) changes induced by the atmospheric forcing anomalies. Off Southern California, climate changes in EKE are key to larvae distribution for commercial species such as the California sardine (*Sardinops sagax*). *Logerwell and Smith* [2001] have described this relationship using historical observations from the CalCOFI program.
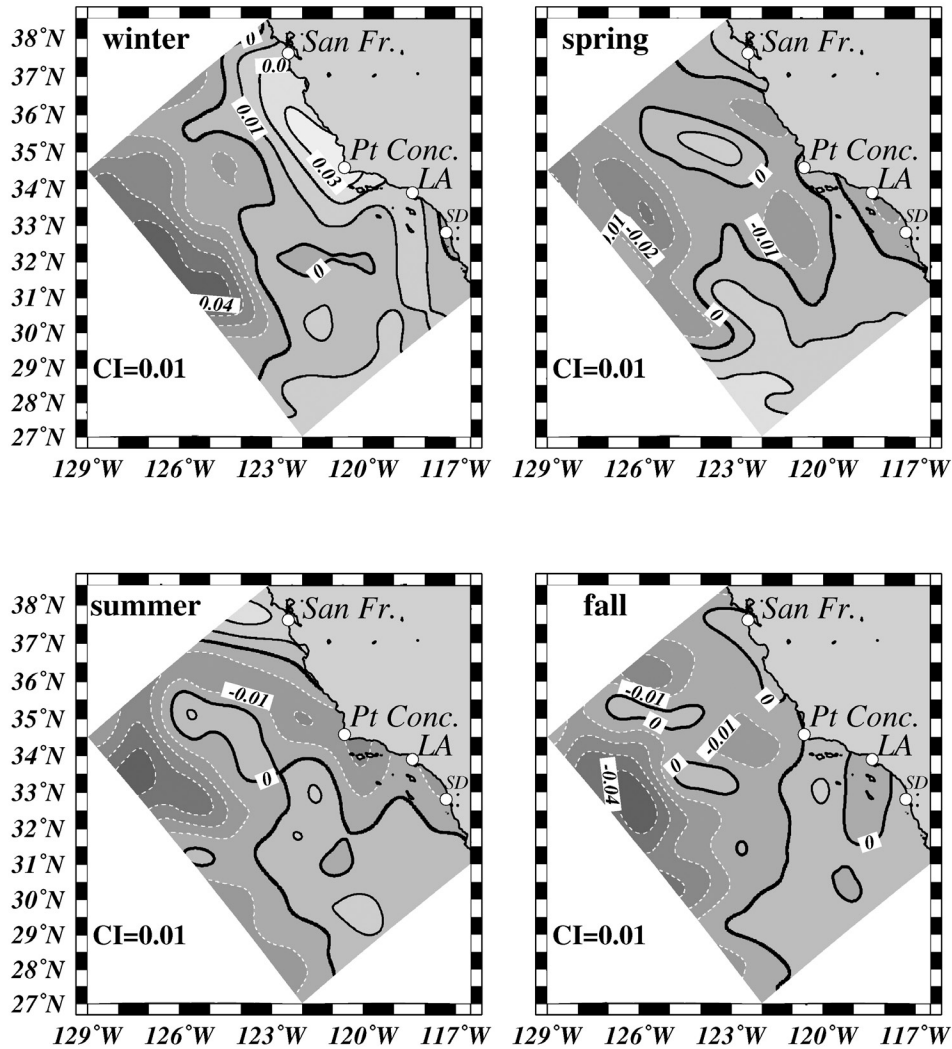
Figure 6. Climatological change in the alongshore component of the flow at 150 m. Units are in m s^{-1}.

[20] The generation of EKE is a complex process involving mean flow stability conditions and nonlinear interactions which are beyond the scope of this article. The main changes in surface EKE take place about three degrees southwestward of Point Conception (Figure 8), an area known for being a transition between different wind regimes [*Dorman and Winant*, 2000]. In winter and spring, and along the CC path, there is a decrease in the EKE all the way from the northwestern corner of our domain to the southeast. Off Southern California, EKE anomalies are very small year-round, while during spring and summer the area of smallest EKE anomalies gets closer to the coast, probably related to the upwelling increase that is reported in the following section. During the Fall, EKE changes seem to be just a transition between summer and winter, with a decrease near the Point Conception area, and small but positive anomalies elsewhere. Quantitatively, summer and fall exhibit smaller anomalies than winter and spring in EKE with the only exception of the coastal ocean between Point Conception and San Francisco which has the largest negative anomalies of all four seasons. This was also

evidenced in additional experiments that included different portions and lengths of our time series, in one case extending our runs for 20 years (instead of 10 years).

3.2.4. Climate Changes in Vertical Velocity

[21] Upwelling events bring cold nutrient-rich waters to the surface, which set in motion a very active food chain including numerous species ranging from microscopic plankton to 15-m-long gray whales. The peak of the upwelling season takes place in April, which we use to report changes in upwelling velocities, because of its larger signal-to-noise ratios; the latter because vertical velocities in ROMS are noisier than other variables, especially in inviscid runs like those ones described in this paper. Figure 9 shows the climatology and climatology change of the model's vertical velocity at 10 m for April. Typical vertical velocity values near the coast are 1 m d^{-1} approximately (Figure 9a), with forecast anomalies ranging between 20 and 40 cm d^{-1} (i.e., changes of 20–40%; Figure 9b). This increase in upwelling and upwelling favorable winds is in line with the findings of *Bakun* [1990], who studied historical observations of wind stress along several coast-
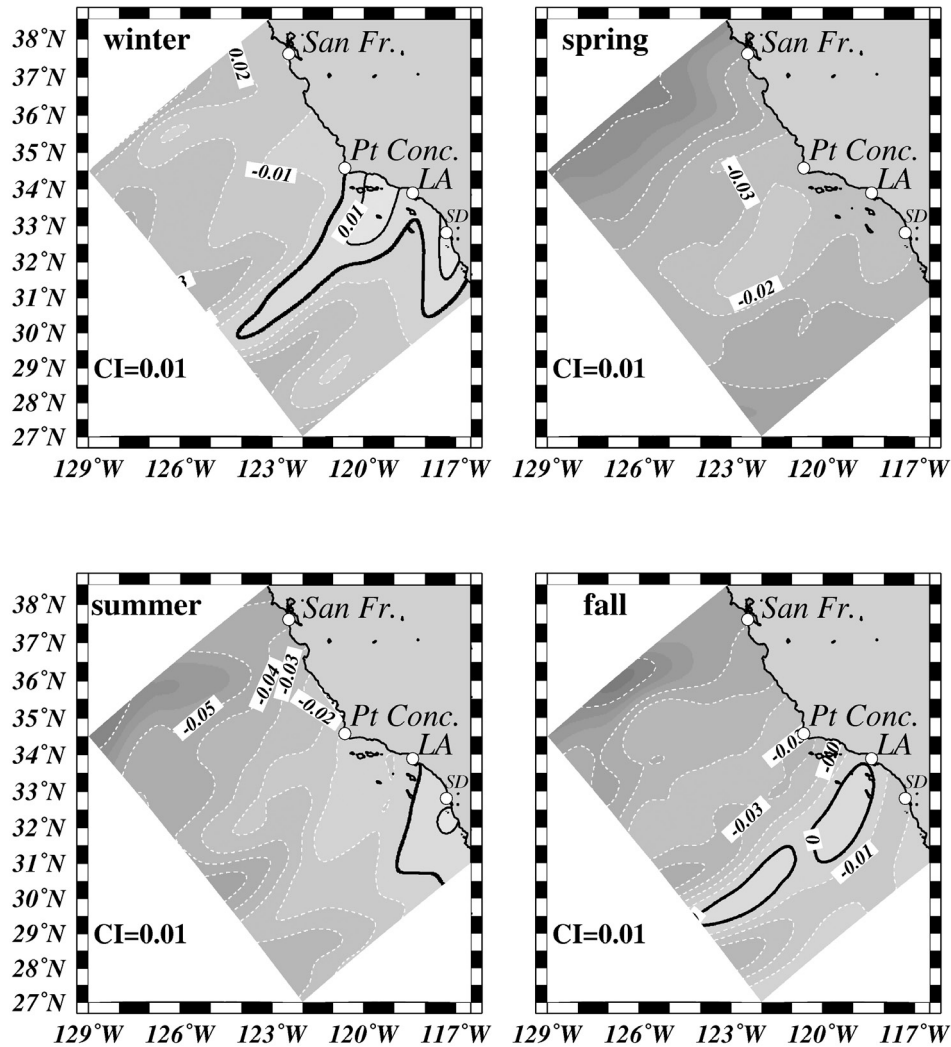
Figure 7. Climatological change in the acrosshore component of the flow at the surface. Units are m s^{-1}.

lines in order to compute global warming trends of alongshore wind stress. It is important to note that vertical velocities are subjected to the competing effects of increased upwelling favorable winds and increased oceanic warming by surface net heat fluxes. The latter tend to increase stratification in the coastal ocean as a function of alongshore distance (Figure 10). Additional experiments with climatological OBCs (not shown) did not show a significant change in the sign and amplitude of vertical velocities (a 5% decrease with respect to Figure 9b).

3.2.5. Climate Changes in Salinity

[22] The increased atmospheric heating has an important effect on the coastal ocean and its biological variables. Changes in salinity concentrations are relevant because below the mixed layer, i.e., away from direct atmospheric influence, they can be regarded as a proxy for nutrients, a key variable in many biological studies. The model forecasts increased coastal salinities at 100 m for every season, and with maximum amplitudes taking place year-round in the northern half of our domain and away from the coastal

ocean (Figure 11). For all four seasons the maximum positive salinities decay toward all boundaries where, in turn, anomalous OBCs are negative year-round at these depths. However, the areas of Figure 11 where the largest positive salinity anomalies take place, approximately coincide with the areas of maximum EKE change shown in Figure 8. This is in line with the recent findings of *Schneider et al.* [2005], who conclude that salinity variations in the California Current are unrelated to climate indexes and their fluctuations. They found that these variations primarily respond to both, advection of the mean meridional salinity gradient by meridional anomalous currents, and to mesoscale variability. Meridional advection is thus ruled out given that the anomalous salinities at the open boundaries are negative for all seasons. Fewer and less intense clockwise-rotating warm eddies could certainly be responsible for inducing an upward salinity transport (or decreasing the downward salinity transport). In addition, a second candidate mechanism, that could reinforce the mesoscale effect, is the vertical advection of the mean
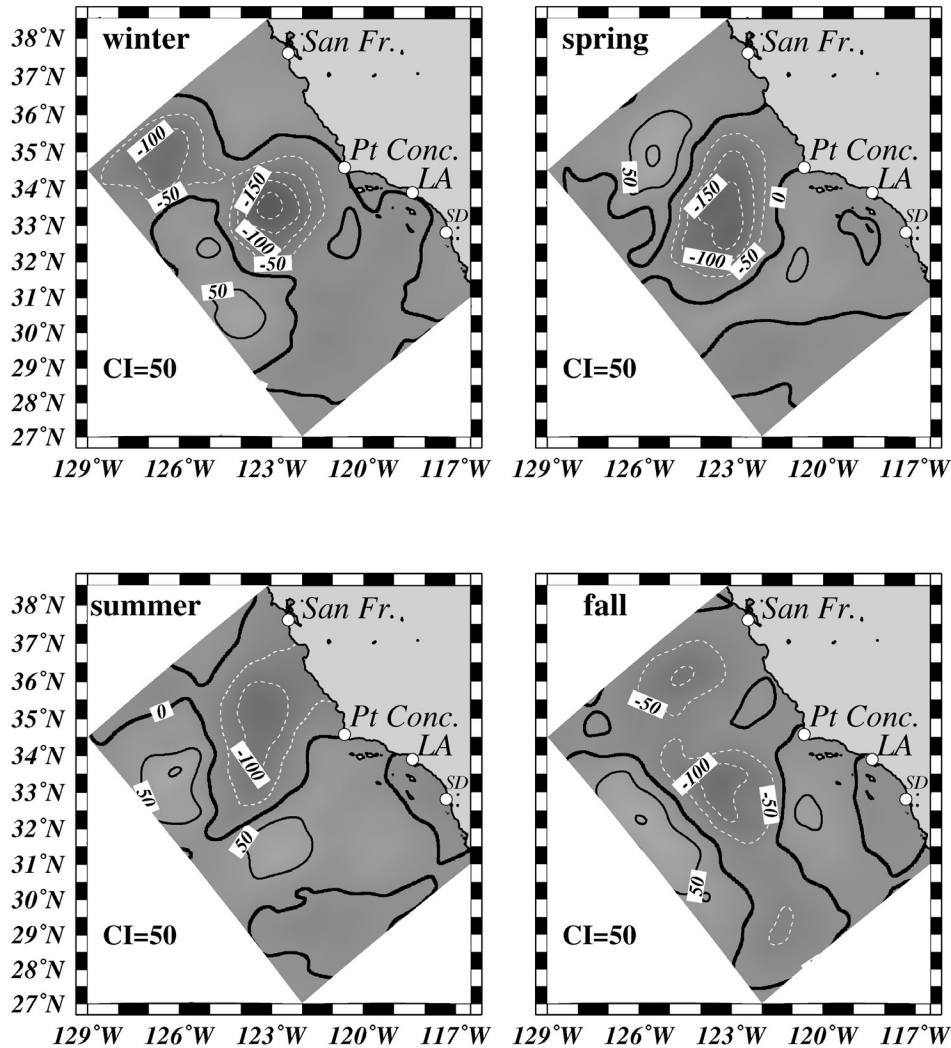
Figure 8. Climatological change in the surface eddy kinetic energy obtained from daily averages. Units are $m^2\ s^{-2}$.

vertical salinity gradient by the climatological change in isopycnal depth (that Figure 3 showed is upward). Figure 11 and similar maps for other depths were constructed (not shown) and indicate that the southern half of our offshore domain exhibits, on average and for all seasons, a negative change in salinity in the 0–100-m-depth range. This is in opposing contrast to the forecast increase in salinity in the northern half (offshore) portion of the CCS.

[23] The run with climatological plus anomalous wind stresses but with climatological heat fluxes only, led to stronger horizontal gradients and larger negative salinity anomalies. This same experiment also led to a slightly smaller vertical displacement of the 26.5 isopycnal surface shown in Figure 3 (mostly in the northern half of our domain), and to a mild deepening of the same surface in the southern half of the domain. Since the EKE in this additional experiment decreases even more than the values shown in Figure 8, we conclude that advection and mixing induced by mesoscale eddies play an important role in leading to the reported positive salinity anomalies. This is also supported by the absence of positive salinity anomalies

in the upper ocean of the coarse resolution PCM. We speculate that the uplifting of the isopycnals (negative anomalies in Figure 3), leads to the creation of positive salinity anomalies in upper levels, while at the same time this increases the amount of available eddy potential energy, thus facilitating the EKE production by baroclinic instability processes. This is supported by the comparison of the extreme values seen in the northern halves of Figures 3, 8, and 11.

[24] The concentration of salinity, among other nutrients, at and near the surface, can play an important factor on the population dynamics of several commercial species. Nutrients in general tend to increase during upwelling events, and this impacts on the local ecosystem, although not always in the same manner [Cushin, 1978]. Many species, for example, the Pacific sardine, have shown significant positive [Walford, 1946] and negative correlations [Marr, 1960] with salinity. This apparent contradiction rises because of the complex interplay among different species, for example, dominance, fishing and size of population in general. For instance, Austin and Ingham [1978]
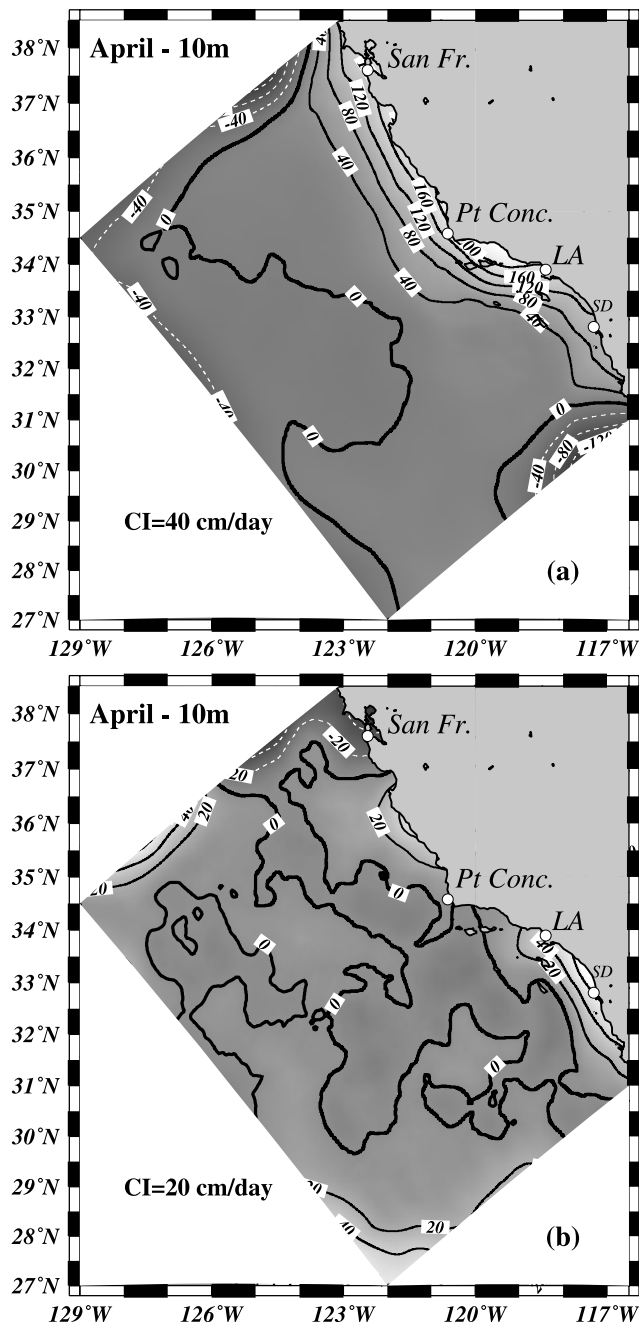
Figure 9. Climatological (a) mean and (b) change of the April vertical velocity at 10 m. (units are cm d^{-1}).

note that a heavily fished stock is likely to be the dominant species and is more responsive to environmental change because it is below its equilibrium density. They further note that the underutilized stock owes its fluctuations to the dominant species rather than to environmental factors. *Bakun* [1973] reported significant correlations between his upwelling index computed off the California coast and abundance of sardine (-0.63) and anchovy ($+0.60$) larvae (a positive correlation implies high salinity and abundance). *Huang et al.* [2006] show that surface salinity and sea surface temperature changes in the CCS area are among the

smallest of the whole Pacific Basin when they force an ocean model with anomalous freshwater forcing.

4. Discussion and Conclusion

[25] Atmospheric warming, a more intense offshore wind field, including a stronger inshore wind stress curl, and anomalous OBCs, lead to a warmer and more stratified upper ocean off California, with increased upwelling velocities in the spring season; dynamically, there is an adjustment in the mass distribution which is characterized by both, higher sea level and shallower isopycnals near the coast during all four seasons. This year-round mass redistribution leads to a generally slower California Current in the southern half of the CCS, and to its acceleration in the northwestern region of the study area. These anomalous currents lead to an anomalous recirculation pattern in the northern half of the domain, which is relevant to the redistribution of nutrients and other biological variables such as larvae concentration. The most biologically relevant forecast is the increase of upwelling velocities near the coast by about 30% in the spring season. However, there will be a tendency for nutrients and larvae to be carried offshore north of the Santa Barbara Channel. South of it, an inshore transport in winter and summer is forecast. Increased upwelling favorable wind stress and increased upwelling favorable wind stress curl (as by *Castelao and Barth* [2006]) team up to overcome an upwelling unfavorable increased stratification. The relative roles of these oceanic and atmospheric processes need to be studied with specifically targeted experiments, higher horizontal resolution and daily forcing in winds and heat fluxes.

[26] By comparing this study to previous published research, we conclude that slow warming trends and rapid warming shifts bear similitudes and differences. In addition to warmer surface and near-surface waters, and increased stratification, rapid warming shifts and slow warming trends result in an anomalous poleward current developing near the coast of the northeastern Pacific Ocean and at around 150-m depth. *Kennett et al.* [2003] described this current taking place during the termination of the last ice age 20,000 years ago, while *Auad et al.* [2003] showed its existence in their modeling solutions of the 1976–1977 warming shift with maximum amplitude in winter. In the current forecast, it is only present as a mild current at about 150 m in winter and with smaller amplitude in fall. On the other hand, recent modeling studies show that isopycnal surfaces deepen in the Northeast Pacific after the 1976–1977 rapid warming shift [*Capotondi et al.*, 2005; *Auad et al.*, 2003], unlike the offshore shallower depths forecast by this study for a slow warming trend. The source of these differences likely lies in the structure of the climatological change of the wind field. In 1976–1977 it shifted to a downwelling favorable pattern, while Figure 1 shows a long-term trend toward a more upwelling favorable scenario.

[27] The forecast EKE has the opposite sign to that one hindcast by *Di Lorenzo et al.* [2005]. Besides the fact that both studies cover different time frames, it is true that the oceanic region under consideration by *Di Lorenzo et al.* [2005] did not cover the time frame of conditions present during the 2040–2050 decade, this under the assumption that the forcing functions used to drive the ocean model are
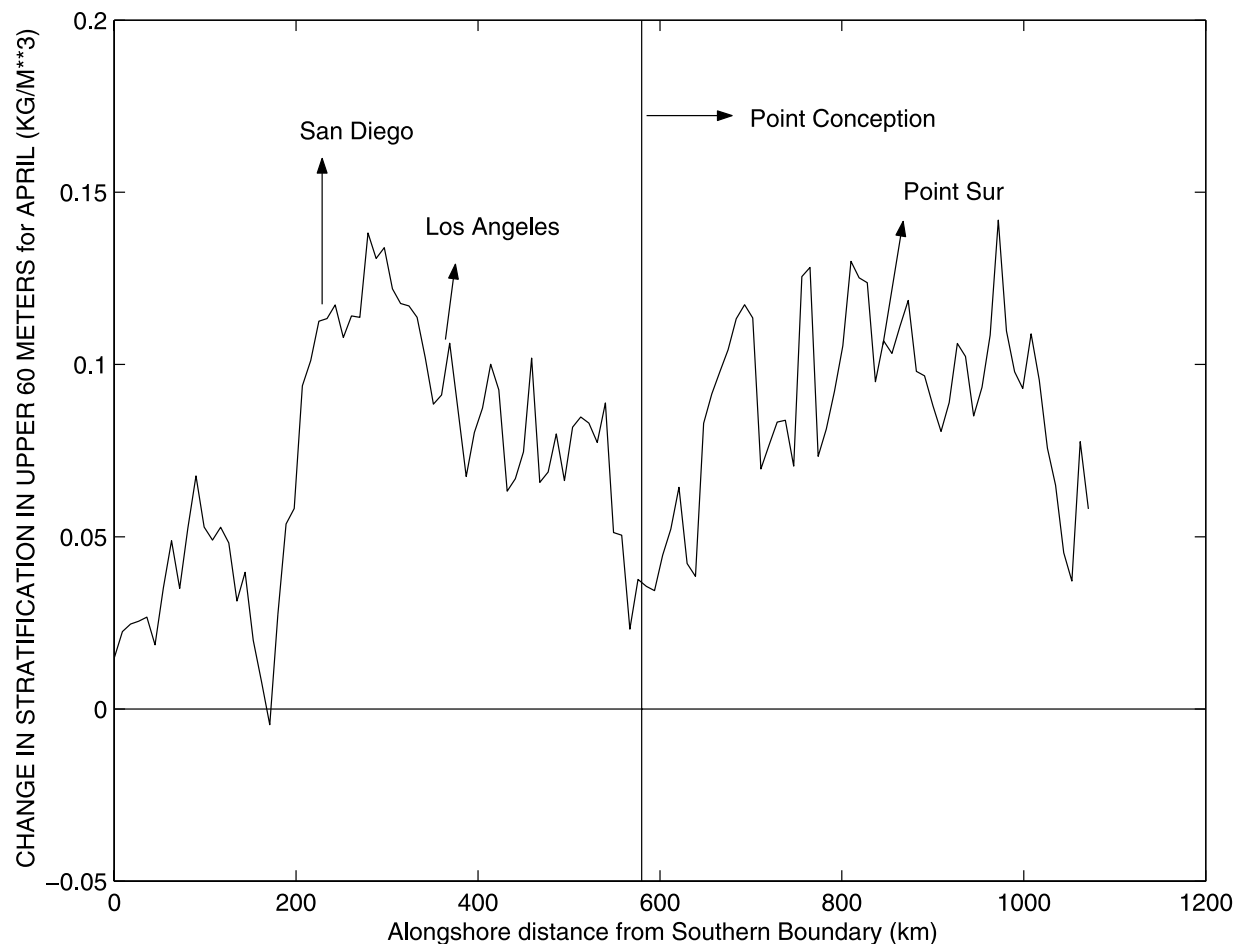
Figure 10. Vertical gradient of density as a function of alongshore distance. The density difference was taken between the surface and the 60 m level and averaged in a coastal band extending 27 km (3 grid points) offshore. Units are kg m^{-3}.

accurate enough. In fact, the average Pacific Decadal Oscillation index (PDO) over the period analyzed by them, 1950–2000, is negative (−0.11), thus suggesting that a more sustained long-term evolution might be necessary in order for the ocean state to evolve to that one forecast here. For example, the temporal evolution of the atmospheric carbon dioxide concentration is nonlinear, especially after the 1960s [*Houghton*, 1997], when it started to rapidly climb. According to him, the carbon dioxide increase for 1950–2000 was about 16%, while that one considered in this study for 1991–2045 is 36%. This difference emphasizes the idea that the global warming changes of the past 50 years are small in comparison to those forecast (here and elsewhere). More specifically, the locations of the maximum wind stress variance change and of the maximum wind stress curl variance change are different in both studies. The latter will certainly have an impact on the underlying mass distribution and circulation.

[28] Our forecast results are in good agreement with those obtained for the slow warming trend of the last half a century by the modeling experiments of *Barnett et al.* [2005] and by the observational studies of *Bakun* [1990], *Schwing and Medelssohn* [1997], and *Palacios et al.*

[2004]. We conclude that these authors and the present study have analyzed different temporal segments of the same global warming trend, although more insight needs to be gained from observations in the near future by specifically computing and studying nonlinear trends, as by *Schwing and Medelssohn* [1997]. The role of the wind stress and wind stress curl anomalies in inducing nonlinear changes in EKE through changes in the ocean's stability properties, also needs to be addressed by future research.

[29] The forecast oceanic changes carry important biological implications given the active fishing that has historically characterized the study area. Our experiments were limited to forecast the intensity of upwelling on a monthly average. However, it remains to be investigated if the number of upwelling events during the spring–summer months will change and how. The forecast increased upwelling velocities will result in nutrient richer waters in the surface and near-surface ocean off California. This has the potential to be enhanced, at least in the subsurface waters, by the forecast shallower isopycnal depths, which lift saltier, nutrient-rich waters. Once at or near the surface, local currents will transport these nutrients and larvae. The only area in which our experiments forecast an increased inshore
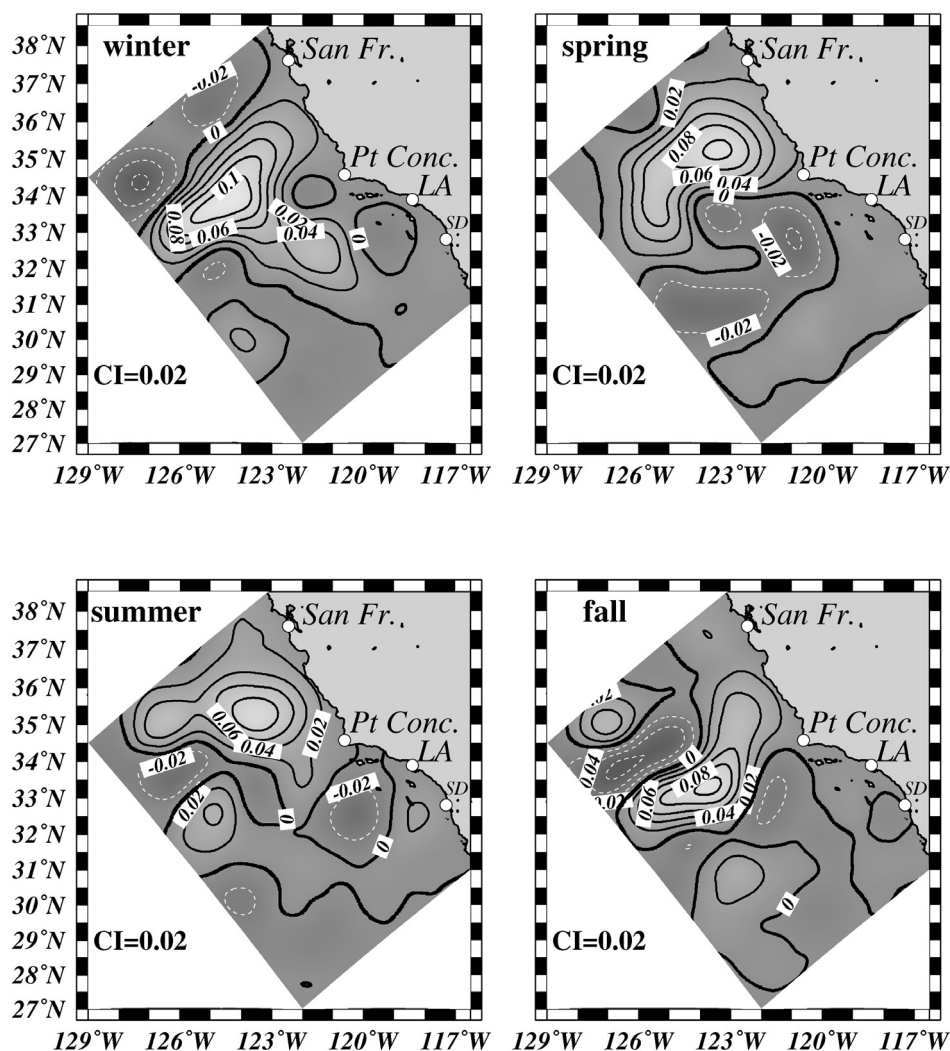
Figure 11. Climatological change in salinity at 100 m. Units are psu.

transport is the southern part of the Southern California Bight, especially in the summer season. The sardine fishing industry/fleet based in San Pedro (south of Los Angeles), California could certainly benefit from these forecast oceanic changes. North of Point Conception the forecast offshore transport would not favor the concentration of nutrients and larvae in the coastal ocean. In addition, the forecast salinity changes indicate that there will be an increase in the concentration of nutrients and larvae about 300 km westward of Point Conception, a location that shows mild seasonal displacements in its geographical position. These increased concentrations are forecast to take place (on a regional average) in the northern half of the study area and in the upper 300 m excluding the coastal ocean. In contrast, in the southern half of the offshore CCS, lower concentrations are forecast with maximum amplitudes at depths centered between 40 and 60 m. In an upcoming study, we will extend our domain to include the active fisheries off Alaska, an area where the forecast global warming trend by the PCM is the largest in the Northeast

Pacific (M. Tyree, personal communication, 2005), and couple a sea-ice model to the ROMS.

References

Auad, G., A. Pares-Sierra, and G. K. Vallis (1991), Circulation and energetics of a model of the California Current System, *J. Phys. Oceanogr.*, *21*, 1534–1552.

Auad, G., A. J. Miller, and W. White (1998), Simulated heat storages and associated heat budgets in the Pacific Ocean: Interdecadal timescale, *J. Geophys. Res.*, *103*, 27,621–27,636.

Auad, G., J. Kennett, and A. Miller (2003), North Pacific Intermediate Water response to a modern climate warming shift, *J. Geophys. Res.*, *108*(C11), 3349, doi:10.1029/2003JC001987.

Austin, H. M., and M. C. Ingham (1978), Use of environmental data in the prediction of marine fisheries abundance, in *Climate and Fisheries*, pp. 89–93, Cent. for Ocean Manage. Stud., Univ. of R. I., Providence.

Bakun, A. (1973), Coastal upwelling indexes, west coast of North America, 1946–71, *U.S. Natl. Mar. Fish. Serv. Tech. Rep. SSRF-671*, 103 pp., Silver Spring, Md.

Bakun, A. (1990), Global climate change and intensification of coastal ocean upwelling, *Science*, *247*, 198–201.

Barnett, T., D. Pierce, K. Rao, P. Glecker, B. Santer, J. Gregory, and W. Washington (2005), Penetration of human-induced warming into the world's oceans, *Science*, *309*, 284–287.

Beamish, R. J. (1993), Climate and exceptional fish production off the west coast of North America, *Can. J. Fish. Aquat. Sci.*, *50*, 2270–2291.

Capet, X., P. Marchesiello, and J. McWilliams (2004), Upwelling response to coastal wind profiles, *Geophys. Res. Lett.*, *31*, L13309, doi:10.1029/2004GL020303.

Capotondi, A., M. Alexander, C. Deser, and A. Miller (2005), Low frequency pycnocline variability in the northeast Pacific, *J. Phys. Oceanogr.*, *35*, 1403–1420.

Castelao, R., and J. A. Barth (2006), Upwelling around Cabo Frio, Brasil: The importance of wind stress curl, *Geophys. Res. Lett.*, *33*, L03602, doi:10.1029/2005GL025182.

Cayan, D. (1992), Latent and sensible heat-flux anomalies over the northern oceans: Driving the sea surface temperature, *J. Phys. Oceanogr.*, *22*, 859–881.

Cushin, D. H. (1978), Climatic variation and fisheries, in *Problems and Progress in Oceanography Relevant to Fisheries*, edited by J. A. Gulland, *FAO Fish. Rep., 206*, suppl. 1, append. 2, 18–19.

Dai, A., and K. E. Trenberth (2002), Estimates of freshwater discharge from continents: Latitudinal and seasonal variations, *J. Hydrometeorol.*, *6*, 660–687.

Di Lorenzo, E., A. J. Miller, N. Schneider, and J. C. McWilliams (2005), The warming of the California Current: Dynamics, thermodynamics and ecosystetm implications, *J. Phys. Oceanogr.*, *35*, 336–362.

Dorman, C. E., and C. D. Winant (2000), The marine layer in and around the Santa Barbara Channel, *Mon. Weather Rev.*, *128*, 261–282.

Han, J., and J. Roads (2004), US climate sensitivity simulated with the NCEP regional spectral model, *Clim. Change*, *62*, 115–154, doi:10.1023/B:CLIM.0000013675.66917.15.

Han, J., H.-M. H. Juang, S.-Y. Hong, M. Kanamitsu, and J. Roads (2000), Experimental simulations with a new NCEP RSM, paper presented at 2nd International RSM Workshop, NOAA, Kihei, Hawaii, July.

Hansen, J. (1998), Book review of Sir John Houghton's *Global Warming: The Complete Briefing*, *J. Atmos. Chem.*, *30*, 409–412.

Hickey, B. M. (1979), The California Current System-Hypothesis and facts, *Progr. Oceanogr.*, *8*, 191–279.

Houghton, J. (1997), *Global Warming: The Complete Briefing*, 251 pp., Cambridge Univ. Press, New York.

Huang, B., V. Mehta, and N. Schneider (2006), Oceanic response to idealized net atmospheric freshwater in the Pacific at the decadal timescale, *J. Phys. Oceanogr.*, *35*, 2467–2486.

Juang, H., S. Hong, and M. Kanamitsu (1997), The NMC nested regional spectral model: An update, *Bull. Am. Meteorol. Soc.*, *78*, 2125–2143.

Kalnay, E., et al. (1996), The NCEP/NCAR 40-year reanalysis project, *Bull. Am. Meteorol. Soc.*, *77*, 437–471.

Kanamitsu, M. (2000), Latest GSM/RSM system, paper presented at Second International Regional Spectral Model Workshop, Maui High Performance Comput. Cent., Maui, Hawaii.

Kennett, J. P., K. G. Cannariato, I. L. Hendy, and R. J. Behl (Eds.) (2003), *Methane Hydrates in Quaternary Climate Change: The Clathrate Gun Hypothesis*, 216 pp., AGU, Washington, D. C.

Levitus, S., R. Burgett, and T. P. Boyer (1994), *World Ocean Atlas 1994*, vol. 3, *Salinity*, *NOAA Atlas NESDIS 3*, 99 pp., Natl. Oceanic and Atmos. Admin., Silver Spring, Md.

Logerwell, E. A., and P. E. Smith (2001), Mesoscale eddies and survival of late stage Pacific sardine (*Sardinops sagax*) larvae, *Fish. Oceanogr.*, *10*, 13–25.

Lynn, R. J., and J. J. Simpson (1987), The California Current System: The seasonal variability of its physical characteristics, *J. Geophys. Res.*, *92*, 12,947–12,966.

MacCall, A. D., and M. H. Prager (1988), Historical changes in abundance of six fish species off southern California, based on CalCOFI egg and larva surveys, *Calif. Coop. Oceanic Fish. Invest. Rep.*, *29*, 91–101.

Marchesiello, P., J. McWilliams, and A. Shchepetkin (2003), Equilibrium structure and dynamics of the California Current System, *J. Phys. Oceanogr.*, *33*, 753–783.

Marr, J. (1960), The causes of major variations in the catch of the Pacific Sardine, in *World Scientific Meeting on the Biology of Sardines and Related Species*, vol. 3, pp. 667–791, Food and Agric. Org., Rome.

Miller, A. J., D. R. Cayan, T. P. Barnett, N. E. Graham, and J. M. Oberhuber (1994), The 1976–1977 climate shift of the Pacific Ocean, *Oceanography*, *7*, 21–26.

Oberhuber, J. M. (1988), An atlas based on the COADS Data Set, *Tech. Rep. 15*, Max-Planck-Inst. fur Meteorol., Hamburg, Germany.

Palacios, D., S. Bograd, R. Mendelssohn, and F. Schwing (2004), Long-term and seasonal trends in stratification in the California Current, 1950–1993, *J. Geophys. Res.*, *109*, C10016, doi:10.1029/2004JC002380.

Roemmich, D., and J. McGowan (1995), Climate warming and the decline of zooplankton in the California Current, *Science*, *267*, 1324–1326.

Schneider, N., E. Di Lorenzo, and P. Niiler (2005), Salinity variations in the California Current, *J. Phys. Oceanogr.*, *35*, 336–362.

Schwing, F., and R. Medelssohn (1997), Increased coastal upwelling in the California Current System, *J. Geophys. Res.*, *102*, 3421–3438.

Song, Y. T., and D. Haidvogel (1994), A semi-implicit primitive equation ocean circulation model using a generalized topography-following coordinate system, *J. Comput. Phys.*, *115*, 228–244.

Walford, L. (1946), Correlation between fluctuations in abundance of the Pacific sardine and salinity of sea water, *J. Mar. Res.*, *VI*, 48–53.

Washington, W., et al. (2000), Parallel Climate Model (PCM): Control and transient simulations, *Clim. Dyn.*, *16*, 755–774.

Watson, W. (1992), Distribution of larval Pacific sardine, *Sardinops sagax*, in shallow coastal waters between Oceanside and San Onofre, California: 1978–1986, *Calif. Coop. Oceanic Fish. Invest. Rep. 37*, 89–99.

————————————————

G. Auad and A. Miller, Scripps Institution of Oceanography, 9500 Gilman Drive, La Jolla, CA 92093, USA. (guillo@ucsd. edu)

E. Di Lorenzo, School of Earth and Atmospheric Sciences, Georgia Institute of Technology, Atlanta, GA 30332-0340, USA.